10. ALPHA PARTICLE SOURCE FUNCTION

The first step in solving (9.19) is determining the initial conditions, i.e. the alpha source rate, at $v = v_o$, where v_o is the birth speed corresponding to 3.5 MeV. This is done by integrating (9.19) over an element of 6-space, $d^3v d^3x$, from $v_o - \Delta v \leq v \leq v_o + \Delta v$, then taking the limit $\Delta v \to 0$. Integrating by parts, and noting that there cannot be an accumulation of particles in any volume element, the result is:

$$f(v_o,\zeta_o,\psi_{xo}) = \tilde{\varepsilon}(v_o,\zeta_o,\psi_{xo})/4\pi\tilde{U}(v_o,\zeta_o,\psi_{xo}). \tag{10.1}$$

The 6-space volume element used above is most easily found through the pair of transformations $(R,z,v,\eta) \to (B,\psi,v,\eta) \to (\psi,\psi_x,v,\zeta)$, yielding

$$d^3v d^3x = (2\pi v^2 dv d\zeta)(2\pi R d\psi_x d\psi)/\mathcal{J}_1\left(\frac{B,\psi}{R,z}\right)\mathcal{J}_2\left(\frac{\psi_x,\zeta}{B,\eta}\right), \tag{10.2}$$

where the Jacobians are

$$\mathcal{J}_1\left(\frac{B,\psi}{R,z}\right) = R|\vec{B}\cdot\nabla B|, \text{ and} \tag{10.3}$$

$$\mathcal{J}_2\left(\frac{\psi_x,\zeta}{B,\eta}\right) = 2B_x^3F[1-\tfrac{1}{2}(1-\zeta^2)B/B_x]/F_xB^3(1+\zeta^2)|B'_{ex}-B'_{ox}|. \tag{10.4}$$

Combining (10.2) - (10.4), $d^3v d^3x$ can be written as:

$$d^3v d^3x = 4\pi v^2 \mathcal{J} dv d\psi_x d\zeta \left(\frac{d\tau'}{d\psi}\right) d\psi, \tag{10.5}$$

where $\mathcal{J}$ is the 'net' Jacobian of the transformation

$$\mathcal{J} = \pi F_x(1+\zeta^2)|B'_{ex}-B'_{ox}|/B_x^3 \ . \tag{10.6}$$

The term $(d\tau'/d\psi)$ is obtained from the bounce-time differential, $d\tau' = d\tau/\left(\frac{2e}{\gamma m v^2}\right)$, where

$$\tau_b = \oint d\tau = 2\int_{\psi_n}^{\psi_x} \frac{d\psi}{|\vec{v}_d\cdot\nabla\psi|} = \frac{2e}{\gamma m v^2}\int_{\psi_n}^{\psi_x} \frac{B^3 d\psi}{F|\vec{B}\cdot\nabla B|[1-B(1-\zeta^2)/2B_x]} \ , \tag{10.7}$$

and $\vec{v}_d$ is the particle guiding-center drift velocity. The extra factor of two in (10.5) and in (10.7) is due to up-down symmetry in $\pm$ z. The remaining problem is to evaluate (10.1).

10.1 Calculation of Integrals

Our calculations are performed as follows. First, a point in (v,ζ,ψ_x) space, corresponding to a particular orbit, is chosen, so as to lie outside the forbidden region defined by (8.4). Next, the sequence of points, $(\psi_o, B_o(\psi_o;v,\zeta,\psi_x))$, are calculated along this orbit between $\psi_n \leq \psi_o \leq \psi_x$. The value of ψ_n is found numerically as the point at which the orbit in B-ψ space crosses the $(B\text{-}\psi)_{EQ}$ curve (c.f. Fig. 8.1a). Third, for each point, (B_o,ψ_o), the corresponding spatial coordinate, (R_o,z_o), is found numerically by solving:

$$\left.\begin{aligned} B_e(R_o,z_o) &= B_o \\ \psi_e(R_o,z_o) &= \psi_o \end{aligned}\right\} \ , \tag{10.8}$$

using the non-linear equation solver HYBRD1[89]. Here, the poloidal flux function for the equilibrium, ψ_e, is found by Lagrangian interpolation of ψ-values given on an (R_i, z_j) mesh. The equilibrium $\vec{B}$-field, $B_e = |\vec{B}_e|$ is similarly found from [85]:

$$\vec{B}_e = \left[-\hat{R}\frac{\partial\psi}{\partial z} + \hat{z}\,\frac{\partial\psi}{\partial R} + \hat{\phi}\;F(\psi)\right] \Big/ R, \text{ so that} \tag{10.9}$$

$$B_e = \sqrt{|\nabla\psi|^2 + F^2} \Big/ R\ . \tag{10.10}$$

Also, at each spatial point on the orbit, $\vec{B}\cdot\nabla B$ is obtained:

$$\begin{aligned}\vec{B}\cdot\nabla B = \frac{1}{BR^4}\frac{\partial\psi}{\partial z}\left[F^2 + \left(\frac{\partial\psi}{\partial R}\right)^2 + \left(\frac{\partial\psi}{\partial z}\right)^2\right] + \frac{1}{BR^3}\Bigg\{\frac{\partial\psi}{\partial R}\frac{\partial\psi}{\partial z}\left(\frac{\partial^2\psi}{\partial z^2} - \frac{\partial^2\psi}{\partial R^2}\right) \\ + \frac{\partial^2\psi}{\partial R\partial z}\left[\left(\frac{\partial\psi}{\partial R}\right)^2 - \left(\frac{\partial\psi}{\partial z}\right)^2\right]\Bigg\},\end{aligned} \tag{10.11}$$

and used to evaluate the integrand of (10.7). Finally, the bounce-averaged quantities $\tilde{s}$ and $\tilde{U}$ in (10.1) are determined numerically (see Appendix E).

10.2 Results

Figure 10.1 shows contours of constant τ_b in (ψ_x, ζ) space for 3.5-MeV alphas in a D-shaped tokamak reactor having $\overline{\beta} = 0.8\%$. In comparing this to Fig. 8.1c, all the features of the phase space topology are present. The prominent aspects include the absence of orbits in the forbidden region (blank portion about $\zeta = 0$ and near

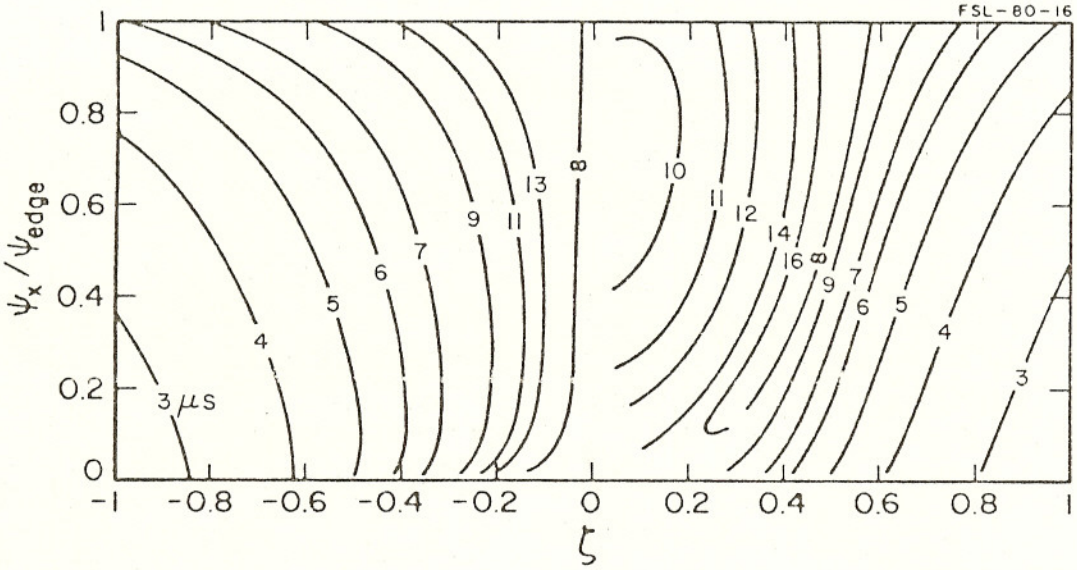

Figure 10.1 Contours of constant bounce time, $\tau_b(\mu s)$, in (ψ_x,ζ) space for 3.5-MeV alphas in a D-shaped tokamak equilibrium ($\overline{\beta}$=0.8%).

$\psi_x/\psi_e = 0$), $\tau_b \to \infty$ along the left-hand side of the forbidden region (for counter-going, x-type stagnation orbits, curve BCD in Fig. 8.1c), the transition to finite τ_b at the end of the pinch locus (point H in Fig. 8.1c), and the transition to finite τ_b at the x-type to o-type stagnation-orbit transition (point B in Fig. 8.1c). Hinton et. al. [98] have examined the transport for particles on or near x-type stagnation orbits and found that a banana-plateau regime model is required, since $\tau_b \to \infty$. Here, we assume that slowing down drifts carry fast ions across such regions rapidly enough that the contribution from plateau-like regimes is small. As expected, circulating ions ($\zeta \to \pm 1$) have the shortest τ_b, since they circulate along an average flux surface. The τ_b-value for circulating orbits ($\zeta \sim \pm 1$) increases with increasing ψ_x because the distance that the ion travels around its average flux surface increases. Also, as expected, $\tau_b \sim 1/v$, even for 3.5-Mev alphas; this is because the distance along the orbit, i.e. the connection length, is essentially independent of v. These features of τ_b in (ψ_x,ζ) space thus reinforce the orbit topology concepts discussed in Chapter 8.

Another set of important results, which are readily calculated at this stage, are the flux-surface-averaged source rates for alpha density and current. At the birth energy, (9.1) becomes:

$$\left.\frac{\partial f}{\partial t}\right|_{v=v_o} = \tilde{\varepsilon} \tag{10.12}$$

from which the flux-surface-averaged alpha source rate, $\langle\dot{n}_\alpha\rangle$ is:

$$\langle\dot{n}_\alpha\rangle = \int \left.\frac{\partial f}{\partial t}\right|_{v_o} d^3v d^3x \Big/ \int d^3x = \int \tilde{s} d^3v d^3x \Big/ \int_{\psi_1}^{\psi_2} d^3x \ , \tag{10.13}$$

and the parallel component of flux-surface-averaged alpha current rate, $\langle\dot{J}_\parallel\rangle$, is:

$$\langle\dot{J}_\parallel\rangle = \int \left.\frac{\partial f}{\partial t}\right|_{v_o} ev\eta \ d^3v d^2x \Big/ \int d^2x = \int \tilde{s} \ ev\eta \ \frac{d^3v d^3x}{2\pi R} \Big/ \int_{\psi_1}^{\psi_2} d^2x. \tag{10.14}$$

The integrals $\int_{\psi_1}^{\psi_2} d^3x$ and $\int_{\psi_1}^{\psi_2} d^2x$ are the volume and area, respectively, between the flux surfaces labelled by ψ_1 and ψ_2, where $d^2x = dRdz = d^3x/2\pi R$. The corresponding integral over $d^3v d^3x$ also requires that the $d\psi$ piece have the limits $\int_{\psi_1}^{\psi_2} \left(\frac{d\tau}{d\psi}\right) d\psi$, with a point-wise source rate, s:

$$s = n_1(\psi) n_2(\psi) \ \langle\sigma v(T(\psi))\rangle_{12} \ \delta(v-v_o)/4\pi v^2 \ . \tag{10.15}$$

Making these substitutions into (10.13)-(10.14) yields:

$$\langle\dot{n}_\alpha\rangle = \int_0^{\psi_e} d\psi_x \int_{-1}^{1} d\zeta \ \widetilde{n_1 n_2 \langle\sigma v\rangle} \ \mathcal{J}(\psi_x,\zeta) \int_{\psi_1}^{\psi_2} \left(\frac{d\tau'}{d\psi}\right) d\psi \Big/ \int_{\psi_1}^{\psi_2} d^3x \ , \tag{10.16}$$

$$\langle\dot{J}_\parallel\rangle = \frac{ev_o}{2\pi} \int_0^{\psi_e} d\psi_x \int_{-1}^{1} d\zeta \ \widetilde{n_1 n_2 \langle\sigma v\rangle} \ \mathcal{J}(\psi_x,\zeta) \int_{\psi_1}^{\psi_2} \left(\frac{d\tau'}{d\psi}\right) \frac{\eta d\psi}{R} \Big/ \int_{\psi_1}^{\psi_2} d^2x. \tag{10.17}$$

These integrals have been evaluated numerically with an error of $\lesssim 1\%$ using 128x128 equal intervals in (ψ_x,ζ) space. We assume a 50-50 D-T plasma with parabolic density profiles:

$$n_D = n_T = n_i(\psi) = n_o[1-.99(\psi/\psi_e)^2] \tag{10.18}$$

The temperature is self-consistently determined from the pressure profile, $p(\psi)$, used to determine the equilibrium:

$$T_i(\psi) = p(\psi)/4kn_i(\psi), \tag{10.19}$$

where k is the Boltzmann constant. The electron density, n_e, is taken as $n_e = 2n_D$; the electron temperature is assumed equal to the ion temperature, T_i. The central temperature was taken at 15 keV, and the corresponding n_o determined from (10.19), with $\langle\sigma v\rangle$ taken from Ref. 32.

Figure 10.2 shows $\langle\dot{n}_\alpha\rangle$ versus ψ/ψ_{edge} for two D-shaped equilibria (See Table 10.1). For comparison, the point-wise source rate, $\dot{n}_\alpha = n_1 n_2 \langle\sigma v\rangle_{12}$, is also plotted. The particle source rate difference, ε, is given in Table 10.1 for each case, where

$$\varepsilon = (\dot{n}_\alpha - \langle\dot{n}_\alpha\rangle)/\langle\dot{n}_\alpha\rangle \ . \tag{10.20}$$

Since $\varepsilon \lesssim 5\%$ for these cases for $\psi/\psi_{edge} \leq 0.4$, it is concluded that the "in-situ" deposition model is adequate for determinations of the total (ion+electron) interior heating. This is because the heating rate goes like $\dot{E} \sim E_o\langle\dot{n}_\alpha\rangle$, where $E_o = \frac{1}{2} mv_o^2$.

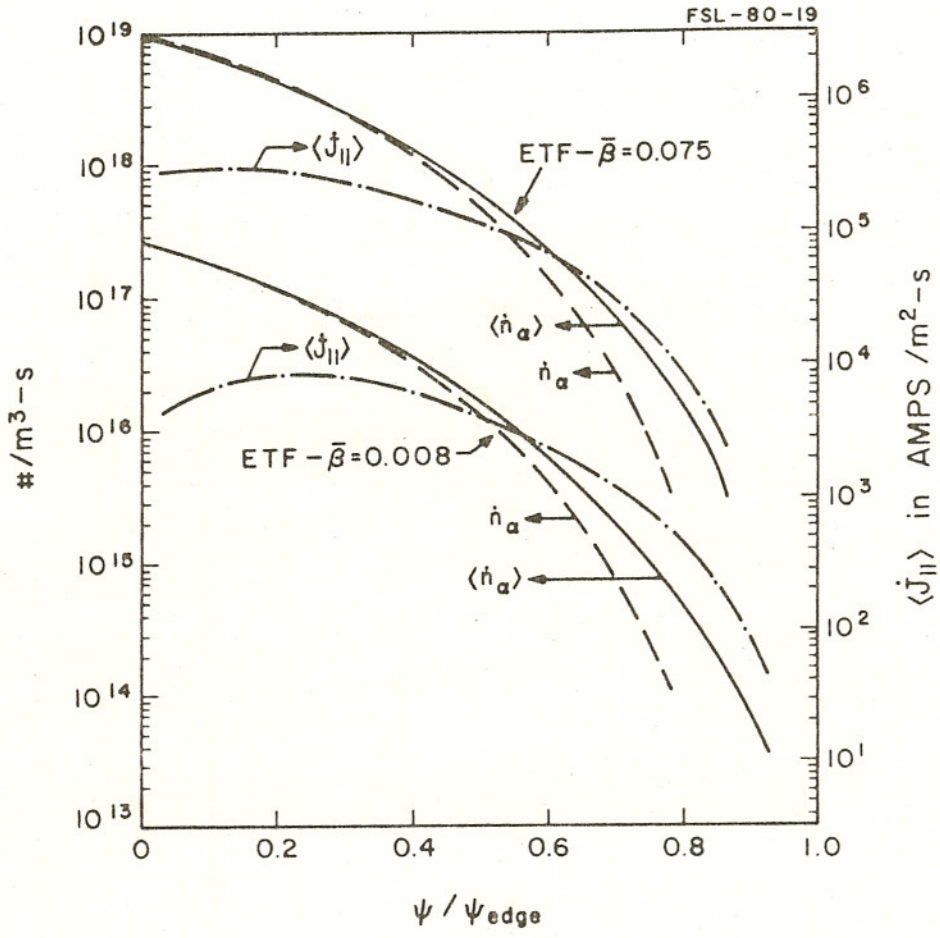

Figure 10.2 Flux-surface-averaged particle source rate, $\langle \dot{n}_{\alpha} \rangle$, and current source rate, $\langle \dot{J}_{\parallel} \rangle$, for 3.5-MeV alphas in D-shaped ETF equilibria (see Table 10.1).

Table 10.1. Non-Circular Tokamak Parameters

	Low β	Medium β	
$\overline{\beta}$	0.008	0.075	given from equilibrium data
$\beta_p(a)$	0.389	2.688	
$q(a)$	3.207	3.353	
J_{pl}(MA)	5.78	5.95	
B_o(T)	5.3	4.3	
R_o(m)	5.035	5.356	
ψ_{edge}(Wb)	3.675	2.985	
ε(%)	4.7	5.4	calculated in present work
$\langle \dot{I}_{\parallel} \rangle$(MA/s)	0.021	0.81	
τ_s(s)	0.9	0.1	
$\tau_s \langle \dot{I}_{\parallel} \rangle$(MA)	0.02	0.08	
$\langle I_{\parallel} \rangle$(kA)*	6.3	26.	

*For a discussion of convergence of $\langle I_{\parallel} \rangle$, see Appendix G.

Figure 10.2 also shows $<\dot{J}_{\parallel}>$ versus ψ/ψ_{edge}, with the values of $<\dot{I}_{\parallel}>$ given in Table 10.1. Small banana-width models are inadequate to describe this current, which is a large banana-width effect. McNally [90] has previously estimated the alpha-driven current using scaling arguments. However, for the purposes of this section, the current is estimated as the current source rate times the characteristic slowing time:

$$I_{\parallel} \sim <\dot{I}_{\parallel}> \tau_s \tag{10.21}$$

where τ_s is the momentum slowing down time (cf. eqn. 11.11). The corresponding estimates for sample cases are given in Table 10.1. In Chapter 11, we improve on this estimate by calculating $<I_{\parallel}>$ as the first moment of the slowing down distribution.